Irradiation of supported gold and silver nanoparticles with continuous-wave, nanosecond and femtosecond laser light: a comparative study

F. Hubenthal[a], M. Alschinger[a], M. Bauer[b], D. Blázquez Sánchez[a], N. Borg[a], M. Brezeanu[a], R. Frese[b], C. Hendrich[a], B. Krohn[a], M. Aeschlimann[b], and F. Träger[a]

[a]Institut für Physik and Center for Interdisciplinary Nanostructure Science and Technology — CINSaT
Universität Kassel, Heinrich-Plett-Str. 40, 34132 Kassel, Germany;
[b]Fachbereich Physik, Technische Universität Kaiserslautern, Erwin-Schrödinger-Str., 67663 Kaiserslautern, Germany

ABSTRACT

Modification of metal nanoparticles with laser light has been a well-known technique for several years. Still, selective tailoring of certain sizes or shapes of nanoparticles has remained a challenge. In this paper, we present recent studies on tailoring the size and shape of supported nanoparticles with continuous-wave and femtosecond pulsed laser light and compare them to our results obtained with ns pulsed laser light. The underlying method is based on the size and shape dependent plasmon resonance frequencies of the nanoparticles. In principle, irradiation with a given laser photon energy excites and heats nanoparticles of certain sizes or/and shapes and leads to diffusion and evaporation of surface atoms. Thus, tailoring the dimensions of the nanoparticles can be accomplished. In our experiments, gold and silver nanoparticles were prepared under ultrahigh vacuum conditions by deposition of atoms and subsequent diffusion and nucleation, i.e. Volmer-Weber growth. This gives particle ensembles with size and shape distributions of approximately 30 % - 40 %. The nanoparticle ensembles were irradiated with laser light either during or after growth. It turns out, that irradiation with cw or ns laser light makes possible selective modification of the nanoparticles. In contrast, application of fs laser pulses results in non-selective modification. For example, post-grown irradiation of supported gold nanoparticles with ns laser pulses ($h\nu = 1.9$ eV) causes a clear reduction of the width of the surface plasmon resonance from 0.52 eV to 0.20 eV (HWHM). Similar experiments were carried out with fs pulsed laser light ($h\nu = 1.55$ eV), which result in a slightly reduced line width but also, to an overall decrease of the extinction. A comparison of all experiments revealed, that for size or shape tailoring of supported metal nanoparticles best results have been achieved with ns pulsed laser light.

Keywords: Laser, gold, silver, nanoparticles, nanostructures, surface-plasmons, tailoring

1. INTRODUCTION

The properties of metal nanoparticles have found a great interest of theoretical and experimental investigations[1–4] due to their unique properties, which bridge the gap between atomic or molecular systems and the bulk material. As a consequence the physical and the chemical properties vary as a function of size and/or shape. Most prominent examples are the size dependent optical properties, catalytic activity and melting point of metals. Especially the optical properties of nobel metal nanoparticles are of general interest, because the optical spectra are dominated by excitations of collective oscillations of the conduction band electrons, namely the surface plasmon resonances, or more precisely speaking by localized surface plasmon polariton excitations. These resonances lead to characteristic extinction peaks in the optical spectra, whose amplitude, position, and

Further author information: (Send correspondence to F.H.)
F.H.: E-mail: hubentha@physik.uni-kassel.de, Telephone: +49 561 804 4501

width in general depend on the size, shape, dielectric surrounding, structure, and material of which the nanoparticles are composed.[4–7] Additionally, the plasmon resonances are associated with a field enhancement in the vicinity of the particle surface, which has been exploited in surface enhanced Raman spectroscopy,[8–10] surface enhanced fluorescence,[11–13] confocal microscopy,[14] and as all-optical switching devices[15,16] or waveguides.[17–19] For optimum interaction of the nanoparticles with a given wavelength, tailor-made nanoparticles of a certain size and/or shape are needed. Therefore, nanoparticles grown by natural Volmer-Weber growth may not guarantee best field enhancement factors and tailoring of the nanoparticles is necessary, which can be done, by means of laser irradiation exploiting the size and shape dependent surface plasmon excitations.[6,20,21]

Manipulation of nanoparticles with laser light has been done quite extensively in the past and different approaches have been used to reshape, melt, or fragment nanoparticles.[22–29] But tailoring selectively the size and/or shape of nanoparticles is still challenging and only a few experiments are dealing with this topic.[6,20,21,30,31] While in most experiments only ns pulsed laser light have been used successfully to tailor supported nanoparticles selectively,[20,21,32–34] detailed investigations about tailoring nanoparticles with cw or fs pulsed laser light are still lacking.

In this contribution we present our first results on tailoring metal nanoparticles with cw as well as fs pulsed laser light. A comparative study of these experiments to our former experiments with ns pulsed laser light[6,21,33,34] is given.

2. NANOPARTICLE PREPARATION

The nanoparticle ensembles were prepared under ultra high vacuum (UHV) conditions (pressure $\leq 5 \cdot 10^{-9}$ mbar) by electron beam evaporation of silver or gold and deposition of the atoms on quartz and sapphire substrates at room temperature. Subsequent diffusion and nucleation, i.e. Volmer-Weber growth leads to an ensemble of nanoparticles with size and shape distributions of approximately 30 % - 40 %.[20,35]

The generated nanoparticles have an oblate shape which can be regarded as rotational ellipsoids. Each particle is characterized by its equivalent radius R_{eq}, i.e. the radius of a sphere with the same volume as the actual non-spherical particle and the axial ratio a/b, a being the short and b the long half axis of the rotational ellipsoid. Due to the growth kinetics, the shape of the nanoparticles depends to their size,[4,36] i.e. the axial ratio drops off when the equivalent radius increases. Only nanoparticles smaller than 1 nm are nearly spherical, while larger nanoparticles have a pronounced oblate shape. It should be noted, that the actual shape depends also on the preparation process, the nanoparticle material and the substrate material. For example, gold nanoparticles display a much smaller value of a/b as compared to silver nanoparticles with the same R_{eq}, supported on the same substrate.

For oblate nanoparticles the surface plasmon resonance splits into two dipole modes, a high-energetic (1,0)- and a low-energetic (1,1)-mode. The (1,0)-mode corresponds to the electron excitation along the short axis and the (1,1)-mode to the direction of the long axis of the rotational ellipsoid. If the axial ratio drops off, the (1,0)-mode shifts to higher and the (1,1)-mode to lower photon energy. If the spectra have been recorded with s-polarized instead of p-polarized light, only the (1,1)-mode can be excited and thus, the (1,0)-mode does not appear. However, in the case of gold nanoparticles, the (1,0)-mode is totally damped by the interband transition of gold starting at approximately 2.4 eV.[37] Thus, only the (1,1)-mode is detectable, independent of the direction of polarization of the light.[4,37–40]

Since the energetic position of the resonances in the size range 1 nm $\leq R \leq$ and 15 nm depends mainly on the shape, i.e. the axial ratio,[4] a size distribution with a typical standard deviation between 30 % and 40 % leads to nanoparticles with different shapes and therefore to inhomogeneous broadening of the surface plasmon resonance.[39–41] For very small ($R \leq 1$ nm) and for large particles ($R \geq 20$ nm) the size influences the position of the modes, too. However, in the size region discussed here (1 nm $\leq R_{eq} \leq$ 15 nm) the position of the resonance depends only on the axial ratio.

3. EXPERIMENTAL

All experiments were accomplished at room temperature. For the preparation of the nanoparticles two different UHV set-ups have been used under similar experimental conditions. Since the experimental results with ns pulsed laser light are presented only for comparison, details of this set-up and the used Nd:YAG laser system can be found elsewhere.[40] The cw and fs laser systems, the UHV and extinction set-ups are described in the following subsections.

3.1. Experimental set-up for the cw laser light experiments

Figure 1 depicts the ultra-high vacuum setup that has been used in these experiments which consists of two chambers: the load-lock chamber and the process chamber with a base pressures of $1 \cdot 10^{-8}$ mbar and $5 \cdot 10^{-10}$ mbar, respectively. An electron beam evaporator (Omicron EMF3) is used to produce a thermal beam of neutral

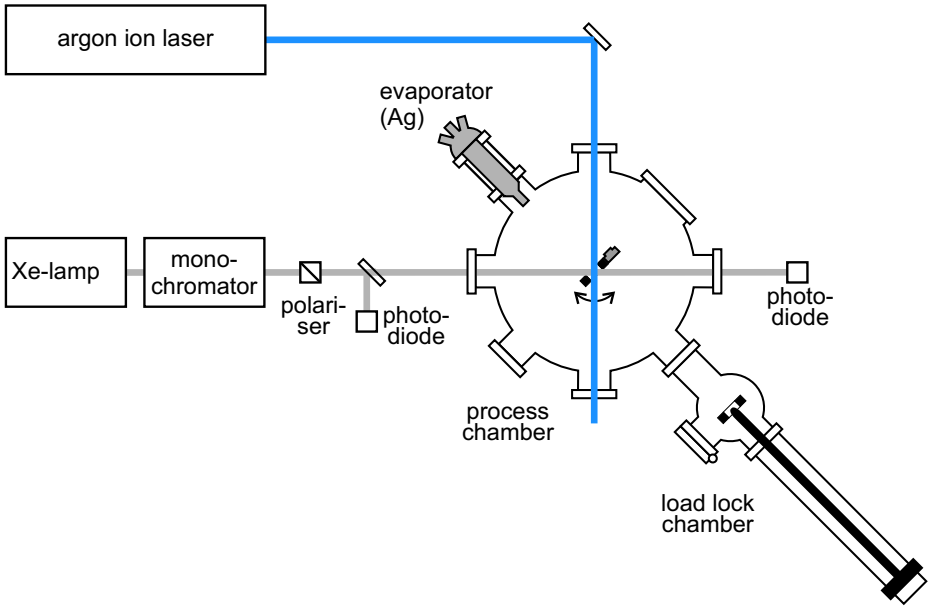

Figure 1. Experimental set-up 1 for nanoparticle preparation and experiments with cw laser light under UHV conditions. For details see text.

silver atoms for preparation of nanoparticles. In addition it is possible to measure the optical spectra of the nanoparticles directly in the UHV system by means of an optical extinction setup.

For tailoring of the nanoparticles a cw argon ion laser has been used (Spectra Physics, 2080E). It provides several laser lines in the blue and green regime of the visible spectrum with an overall intensity of 20 W. In the experiments described here the two most intensive laser lines at $\lambda = 514$ nm (2.41 eV) and $\lambda = 488$ nm (2.54 eV) have been chosen.

3.2. The fs laser system

The irradiation with fs pulsed laser light has been done under ambient conditions. The used gold nanoparticle ensembles have been produced in the experimental set-up described elsewhere[40] and were then transferred to the fs laser system. The fs-laser system consists of a Kerr mode-locked Ti:Sapphire oscillator (KMLabs MTS), pumped by a frequency doubled cw Nd:YVO4 laser (Spetcra-Physics Millenia), that generates 27 fs pulses centered at 797 nm (bandwidth 80 nm (FWHM)) at a repetition rate of 92 MHz. These pulses are then temporally stretched, subsequently seeded into an eight-pass Ti:sapphire amplifier (Quantronix Odin), pumped by a frequency-doubled Q-switched Nd:YLF laser (Quantronix 527DQ), and finally re-compressed into femtosecond pulses. The final output of the laser system is 40 fs pulses at a 1 kHz repetition rate with 1.5 mJ/pulse.

3.3. Extinction set-up

For all experiments the optical spectra were recorded with the light of a Xe-arc lamp (Osram, XBO 450 W/1) in combination with a monochromator (Amko, 600 lines/mm, blaze: 400 nm). We use either p-polarized light with an angle of incidence of 45° or s-polarized light with an angle of incidence of 90°. For the experiments with cw and ns laser light, all spectra have been recorded under ultra high vacuum conditions. Only for the experiments with fs laser light we recorded the spectra with an extinction set-up in ambient conditions, because no UHV set-up was available for the fs laser pulse experiments.

4. NANOPARTICLE CHARACTERIZATION

To characterize the shape and size of the nanoparticles we use a combination of scanning force microscopy (ThermoMicroscopes, Autoprobe CP, AP-0100), optical spectroscopy, and theoretical modelling using the quasistatic approximation[4] with the optical constants of silver[42] and gold,[37] as demonstrated by Wenzel et al..[36]

4.1. Determination of $< R_{eq} >$ and $< a/b >$

The mean equivalent radius $< R_{eq} >$ of the nanoparticle ensembles has been determined by measuring the amount of deposited atoms with a quartz micro balance and counting the nanoparticle number density out of the AFM images. Fig. 2a) depicts a typical AFM image of silver nanoparticles with $< R_{eq} > = (6 \pm 1)$ nm on a quartz substrate. The ensemble exhibits a size distribution of 27 % (fig. 2b), determined from the AFM image.

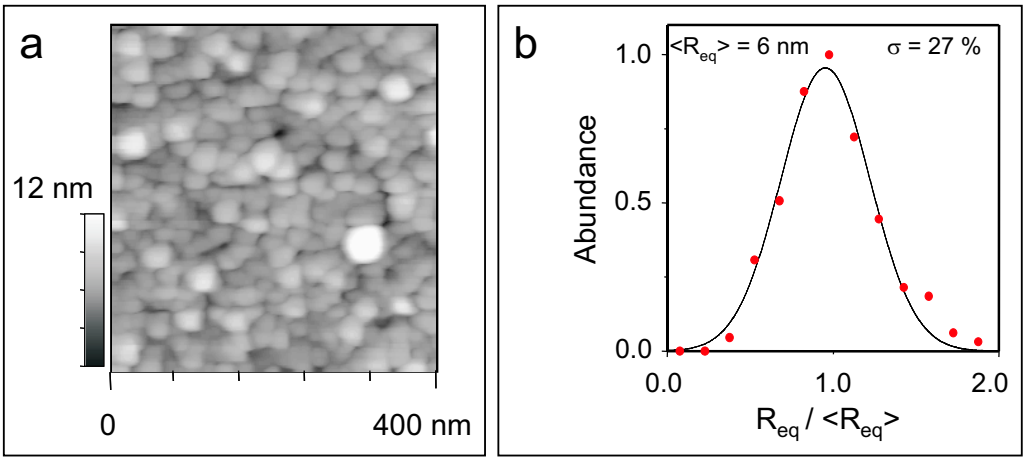

Figure 2. Atomic force microscope image (a) and the corresponding size distribution (b) of silver nanoparticles with $< R_{eq} > = 6$ nm supported on a quartz substrate.

Because of the overestimation of the lateral size of the nanoparticles by AFM, the shape cannot be deduced from these images alone. To determine the shape, we use electrodynamic theory in quasistatic approximation[4] to model the experimental spectra. Since in the size range 1 nm $\leq R_{eq} \leq$ 15 nm the position of the SPR does not depend on the size, the axial ratio a/b of the nanoparticles can be determined by using a/b as a fit parameter in the theoretical modelling. Fig. 3a shows typical extinction spectra for silver nanoparticles on a quartz substrate as a function of photon energy for coverages ranging from $1.5 \cdot 10^{15}$ $\frac{\text{Ag atoms}}{\text{cm}^2}$ to $37.5 \cdot 10^{15}$ $\frac{\text{Ag atoms}}{\text{cm}^2}$. Since the axial ratio decreases while the mean equivalent radius of the nanoparticles increases as depicted in fig. 3b, the (1,1) mode is shifted to lower and the (1,0)-mode to higher photon energies.

5. PRINCIPLES OF TAILORING NANOPARTICLES WITH LASER LIGHT

The underlying method is based on the size and shape dependent plasmon resonance frequencies of metal nanoparticles. In principle, irradiation with a given laser photon energy excites and heats nanoparticles of certain sizes or shapes and leads to diffusion and evaporation of surface atoms. Shining in laser light either during or after growth allows a selective tailoring of the dimensions of the nanoparticles.

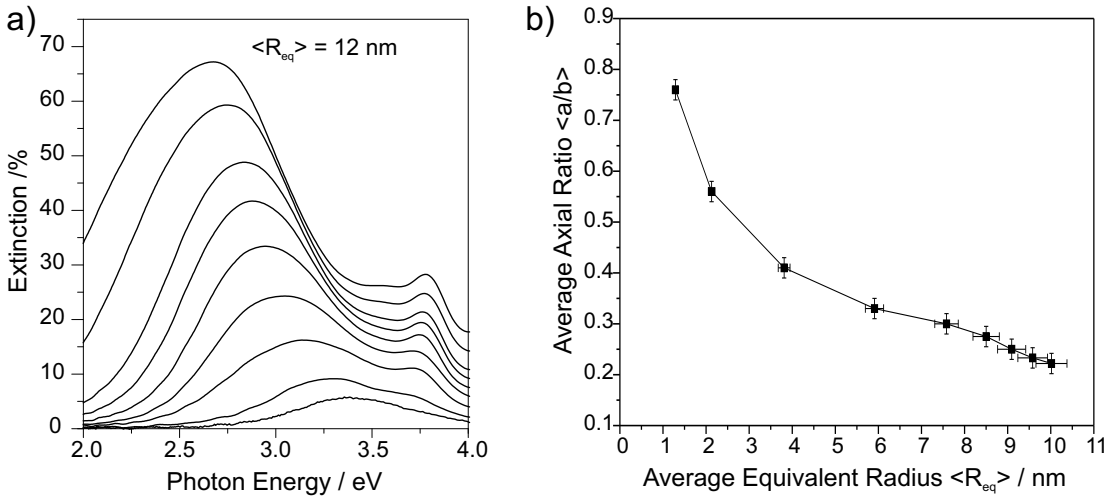

Figure 3. a: Optical spectra of silver particles as a function of the photon energy for coverages ranging from $1.5 \cdot 10^{15}$ $\frac{\text{Ag atoms}}{\text{cm}^2}$ to $37.5 \cdot 10^{15}$ $\frac{\text{Ag atoms}}{\text{cm}^2}$. The shift of both modes for increasing coverage is clearly visible.
b: Mean axial ratio as a function of the mean equivalent radius. Due to the growth kinetics, nanoparticles become more and more oblate for larger sizes.

5.1. Basic idea of shape tailoring

To tailor the shape of nanoparticles cw and ns pulsed laser light was used. The basic idea of this process is depicted in fig. 4a-4c. As mentioned above, the axial ratio of the nanoparticles decrease with increasing size. As

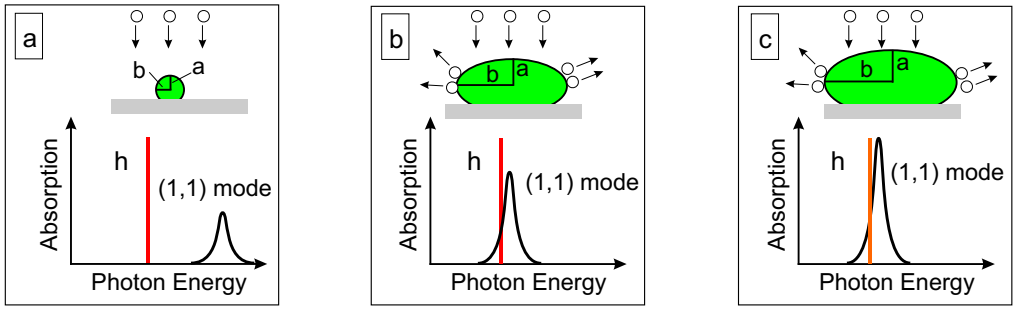

Figure 4. Schematic illustration of the laser assisted growth of metal nanoparticles with predetermined axial ratio.

a consequence, the plasmon resonance frequency shifts to lower photon energy. Thus, the photon energy of the laser light can be chosen such that only nanoparticles with a certain axial ration a/b absorb the light efficiently due to an overlap of the extinction profile and the laser photon energy. The absorbed energy is converted rapidly into heat and self-diffusion and, if the fluence is high enough, evaporation of atoms occur. Since, the atoms are preferentially ejected from places with low coordination numbers, i.e. from the edges of the long axis of the nanoparticles, and due to self diffusion, the axial ratio increases. This leads to a competitive process in which the decrease of a/b because of the growth kinetics is prevented by its increase due to the laser irradiation. As a result, a/b, i.e. the shape of the nanoparticles remains unchanged although the mean size grows (fig. 4c). In this self-regulating process the laser photon energy acts as a barrier that the nanoparticle excitation mode cannot cross. A great advantage of this method is, that the choice of the laser photon energy determines the axial ratio of the particles. Thus, the axial ratio of the nanoparticles can be chosen, simply by varying the photon energy of the laser.[6, 20, 21]

5.2. Basic idea of size tailoring

The principle of tailoring the size of supported metal nanoparticles is schematically illustrated in fig. 5. As

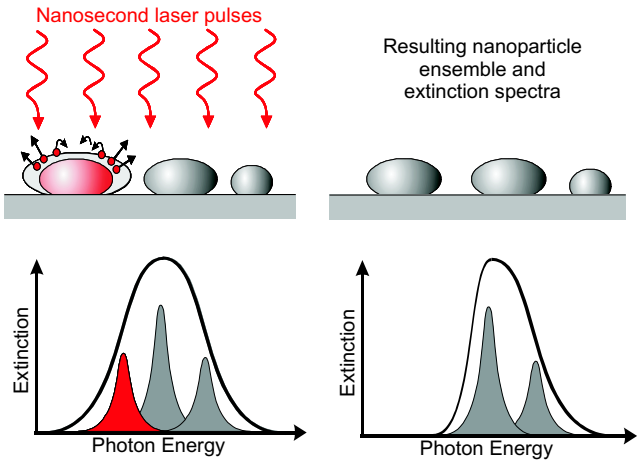

Figure 5. Schematic illustration of the laser based size tailoring of metal nanoparticles.

mentioned above, a nanoparticle ensemble exhibits a size and shape distribution and the plasmon resonance frequency of each single nanoparticle depends on its shape. Irradiation with a certain laser photon energy excites particles with a specific axial ratio only. Contrary to the irradiation during growth, where the laser photon energy has just a small overlap with the extinction profiles and the amount of absorbed energy is small, irradiation after deposition leads to a perfect overlap of the laser photon energy and the extinction profile of the addressed nanoparticles. Thus, for large fluences, the absorbed energy causes a temperature rise, sufficient high that atoms are evaporated from the nanoparticles surface, resulting in a selective modification of the nanoparticle ensemble, within a narrow interval of sizes.

6. RESULTS

In section 6.1 we describe the shape tailoring of the nanoparticles with cw laser light and in section 6.2 experiments in order to tailoring the size of gold nanoparticles with fs pulsed laser light. The results of these experiments are compared with our former results obtained with ns pulsed laser light.

6.1. Tailoring the shape of silver nanoparticles with cw laser light

For the shape stabilization, the nanoparticle ensembles were irradiated during growth with the cw light of an argon ion laser with photon energies of 2.54 eV and 2.41 eV* with a power of 1.5 W. Fig. 6 (left) depicts the resulting extinction spectra for coverages from $1.5 \cdot 10^{15}$ $\frac{\text{Ag atoms}}{\text{cm}^2}$ to $37.5 \cdot 10^{15}$ $\frac{\text{Ag atoms}}{\text{cm}^2}$ if the nanoparticles are irradiated during growth with 2.54 eV. For low coverages ($\leq 3.75 \cdot 10^{15}$ $\frac{\text{Ag atoms}}{\text{cm}^2}$) there is no overlap between the laser line and the extinction profile of the nanoparticles. Therefore, the extinction positions and the amplitudes are identical of those particles grown without laser irradiation (comp. fig. 3a). In contrast, for coverages between $7.5 \cdot 10^{15}$ $\frac{\text{Ag atoms}}{\text{cm}^2}$ and $22.5 \cdot 10^{16}$ $\frac{\text{Ag atoms}}{\text{cm}^2}$ pronounced differences in the optical spectra of the irradiated compared to the non-irradiated nanoparticle ensembles can be seen: The plasmon modes start to be stabilized. Thus the shift of the plasmon modes is smaller than for non-irradiated ensembles. For coverages larger than $26.3 \cdot 10^{16}$ $\frac{\text{Ag atoms}}{\text{cm}^2}$ both plasmon modes remain fixed at photon energies of 3.0 eV and approximately 3.7 eV, i.e. $a/b = 0.48$. We conclude, that using cw laser light during growth indeed stabilizes the surface plasmon resonance frequency,

*Here, we discuss only the results for irradiation with 2.54 eV, because the results with 2.41 eV are completely analogous, only the surface plasmon resonance has been stabilized at a lower photon energy of 2.9 eV, corresponding to an axial ratio of $a/b = 0.38$.

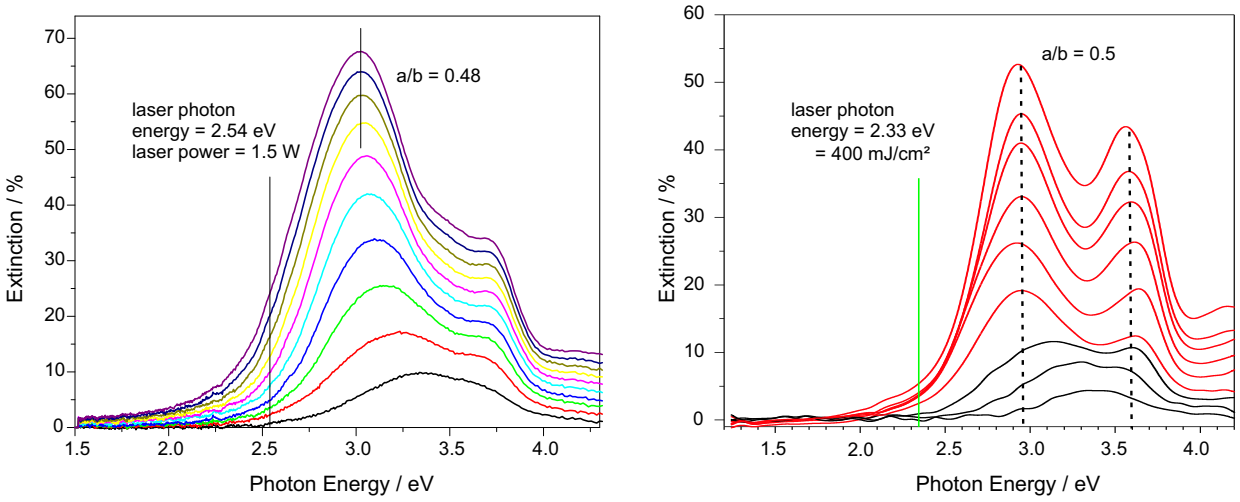

Figure 6. Extinction spectra of silver nanoparticles on quartz substrates, prepared by laser assisted growth with cw laser light (left) and the comparison to similar experiments revealed with silver nanoparticles supported on sapphire irradiated with ns laser light (right).

i.e. the shape of the nanoparticles. However, the size continues to increase and the extinction amplitude rises up to approximately 70 %.

A detailed comparison of these results with our earlier results obtained with silver nanoparticles supported on sapphire substrates and irradiated with ns pulsed laser light (fig. 6, right) reveals some major differences:

- The extinction at the photon energy of the laser light is significant higher if cw laser light instead of ns pulsed laser light has been used,
- the line width of the extinction spectra are broader and more symmetric,
- the maximum of extinction is higher, and
- the stabilization process starts at higher coverage compared to the experiments with ns pulsed laser light.

The reasons for these differences are discussed in section 7.1.

Additionally, the (1,0)-mode in fig. 6 (left) is less pronounced compared to fig. 6 (right). This difference is simply caused by the different substrate materials. Quartz has a lower refractive index compared to sapphire. Thus, the (1,0)-mode lies at higher photon energies, i.e. closer to the interband transition. This causes a more effective damping of the (1,0)-mode for nanoparticles supported on quartz substrates.

6.2. Tailoring the size of supported gold nanoparticles with fs pulsed laser light

Tailoring of the size of gold nanoparticles on quartz substrates with fs laser pulses, has been done under ambient conditions. The wavelength of the Ti:sapphire was set for all experiments to 800 nm, corresponding to a photon energy of 1.55 eV. The applied pulse energy per cm^2 has been varied between 3.19 $\frac{J}{cm^2 \cdot pulse}$ and 4.29 $\frac{J}{cm^2 \cdot pulse}$. The spot size of the laser beam on the sample was 3 mm. The number of applied pulses were varied from 100 to 100000, but no dependence on the pulse rate could be found. Therefore, all following results are obtained with pulse rates between 1000 and 10000. Fig. 7 depicts the optical spectra of gold nanoparticles before (top, left) and after (top, right) laser irradiation with pulse energies per square centimeter of 4.29 $\frac{J}{cm^2 \cdot pulse}$, 3.19 $\frac{J}{cm^2 \cdot pulse}$ and 3.57 $\frac{J}{cm^2 \cdot pulse}$ for the sample numbers 1, 2, and 3, respectively. After irradiation we obtain for all extinction spectra a narrowing of the half width at half maximum HWHM. We found, that the narrowing depends on the applied pulse energy per cm^2. For the nanoparticles irradiated with fs pulses with 4.29 $\frac{J}{cm^2 \cdot pulse}$ a narrowing of the HWHM from approximately 0.60 eV to 0.47 eV has been measured, i.e. a narrowing of 0.13 eV. The narrowing for nanoparticles irradiated with fs pulses with 3.57 $\frac{J}{cm^2 \cdot pulse}$ and with 3.19 $\frac{J}{cm^2 \cdot pulse}$ was only 0.07 eV and 0.05 eV, respectively. In addition we measured an overall decrease in all extinction spectra, which is different compared to our former results, obtained with ns pulsed laser light and depicted in fig. 7 (bottom), for

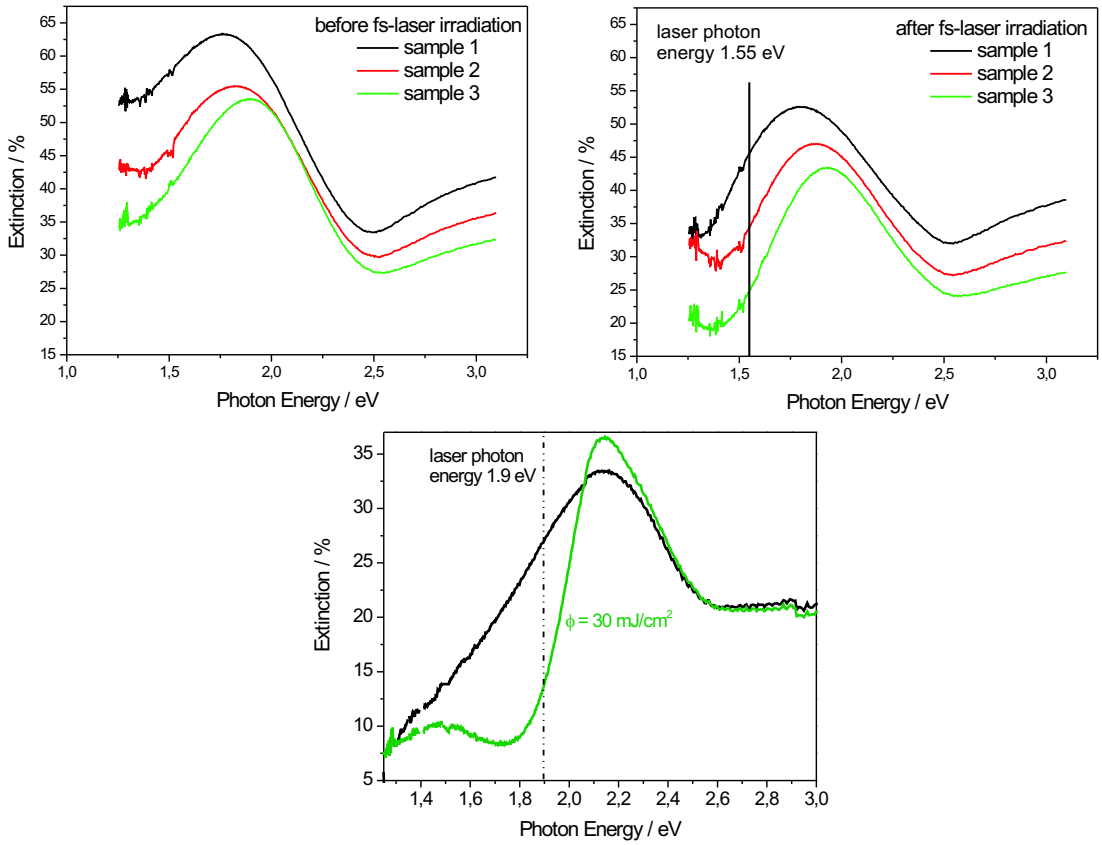

Figure 7. Top: Extinction spectra of gold nanoparticles on quartz substrates, before and after irradiation with fs pulsed laser light with 4.29 $\frac{\mathrm{J}}{\mathrm{cm}^2 \cdot \mathrm{pulse}}$, 3.19 $\frac{\mathrm{J}}{\mathrm{cm}^2 \cdot \mathrm{pulse}}$ and 3.57 $\frac{\mathrm{J}}{\mathrm{cm}^2 \cdot \mathrm{pulse}}$ for the sample numbers 1, 2, and 3, respectively. Bottom: Extinction spectra of gold nanoparticles on quartz substrates, before and after irradiation with ns pulsed laser light with 1.9 eV and a fluence $\phi = 30\ \frac{\mathrm{mJ}}{\mathrm{cm}^2}$.[33]

comparison. Irradiation of nanoparticle ensembles with ns pulsed laser light ($h\nu = 1.9$ eV) leads to a selective tailoring of the resonant nanoparticles and to a significant narrowing of the line width from 0.52 eV to 0.2 eV.[33] Furthermore, an increase of the extinction at higher photon energies is observed, indicating that the surface plasmon resonance of the excited nanoparticles have altered their size and shape towards smaller and more spherical nanoparticles.

7. DISCUSSION

7.1. Tailoring the shape

As presented in section 6.1 cw laser light can be used to tailor the shape of the nanoparticles. But in comparison to similar experiments with ns pulsed laser light, some differences can be seen. The extinction amplitude at the photon energy of the applied laser light is significant higher if cw laser light instead of ns pulsed laser light has been used. Although, the overall deposited energy was in the same order, the temperature rise in the nanoparticles during the illumination time is significant different if cw or ns pulsed laser light is applied. For both cases, the temperature rise is determined by the absorbed energy, the heat transfer from the nanoparticle to the substrate and the thermal conductivity of the substrate.[43] In the case of irradiation with cw light the deposited energy per time is relatively low and can be effectively transferred into the substrate. Therefore, the

temperature rise in the nanoparticles is significant lower and leads to a less effective tailoring process compared to nanoparticles irradiated with ns pulsed laser pulses. In addition, the energy transfer from the nanoparticle leads to an overall heating of the substrate, which causes a non-selective change of the shape of all nanoparticles towards more spherical shape.

In the case of nanoparticles irradiated with ns pulsed laser light the photon energy is deposited within only 5 ns. Compared to the cw laser light experiments the temperature rise in the nanoparticles within 5 ns is much higher, resulting in an increased diffusion and evaporation of atoms of nanoparticles. Due to the fact, that atoms evaporate preferentially from the edges, i.e. from the long axis of the nanoparticles, the axial ratio of the excited nanoparticles is effectively decreased. Additionally, evaporation of atoms leads to a cooling of the nanoparticles. Thus, less energy is transferred into the substrate and only the shape of nanoparticles with predetermined axial ratios, i.e. surface plasmon resonance energies which coincidence with the laser photon energy is altered. This is indicated by the slightly asymmetric surface plasmon resonance and the smaller line width of the nanoparticle ensembles irradiated with ns pulsed laser light (fig. 6, right). Comparing the extinction amplitudes of both experiments, it can be seen, that significant more atoms are evaporated during irradiation with ns pulsed laser light than with cw laser light. The line width and the amplitude of the extinction profile of the nanoparticle ensembles irradiated with cw laser increase nearly to the same values as for un-irradiated nanoparticles (fig. 3 a), while for nanoparticles ensembles irradiated with ns laser pulses a significant lower extinction amplitude and line width is measured, although nearly the same amount of silver has been deposited.

7.2. Tailoring the size

For interpretation of the results obtained with fs pulsed laser light one has to take in account, first, that the bandwidth of the laser is much broader as compared to the ns laser pulses, second, that the experiments have been carried out under ambient conditions and that non-thermal processes can occur.[28–30, 44, 45]

Due du the relatively large bandwidth of the output pulses of the fs laser system of approximately 50 nm (FWHM) compared to the negligible bandwidth of the ns laser system, one would not expect a perfect selectivity of the fs pulsed laser light. Nevertheless, tailoring of nanoparticles is possible and narrowing of the line width and a significant reduction of approximately 35 % of the extinction amplitude at the laser photon energy of $h\nu$ = 1.55 eV for all samples were measured (sec. 6.2). However, for photon energies ranging from 2.0 eV to 3.0 eV a decrease of the extinction amplitude of 10 % took place, which can not be explained by the bandwidth of the fs laser system. Furthermore, a reduction caused by the presence of ambient conditions during illumination e.g. because of oxidation of the nanoparticles is unlikely, because gold nanoparticles do not tend to oxidize.

The main difference compared to ns pulsed laser light is, that non-thermal effects can take place.[23, 27–30, 45] While for ns pulsed laser light the energy absorption, the temperature rise and the heat transfer into the substrate can be explained fully thermodynamically, a thermal equilibrium in the nanoparticles cannot be established during a fs laser pulse, because the pulse length is much shorter than the thermalization time of the nanoparticles which is in the order of picoseconds.[46–49] Therefore, non-thermal processes are very likely in the nanoparticles which may lead to Coulomb fragmentation and/or ablation.[28, 29, 44] Due to the high excitation energy a significant amount of electrons can be ejected from the nanoparticles. This creates highly charged particles, which fragment and/or ablate from the substrate due to a Coulomb explosion and may influence larger areas on the the substrate. The ablated nanoparticles can form larger agglomerates in the size range of several tens up to hundreds of nanometer, which are redeposited on the substrate again. To proof this hypothesis, AFM measurements have been carried out. Figure 8 depicts an image of an area of nanoparticles irradiated with fs laser pulses and the corresponding height profile. Blank areas can bee seen as well as larger aggregates, which have been formed due to coalescence. The height profile clearly shows, that in the black areas no particles are left on the substrate, but also, that the ablation process effects relatively large areas of several hundreds of nanometer. Thus, the ablation influences all sizes of nanoparticles on the substrate and explains the overall reduction of the extinction amplitude. Interestingly, small and obviously unchanged nanoparticles in the vicinity of the ablated areas remained on the substrate.

However, not in all irradiated areas the ablation occurs. In some areas large nanoparticles similar to the ones that can bee seen in fig. 8 were found on a closed layer of unchanged nanoparticles without any blank areas. Additionally, coalescence and reshaping took place and nanoparticles in the size range of several 100 nanometers

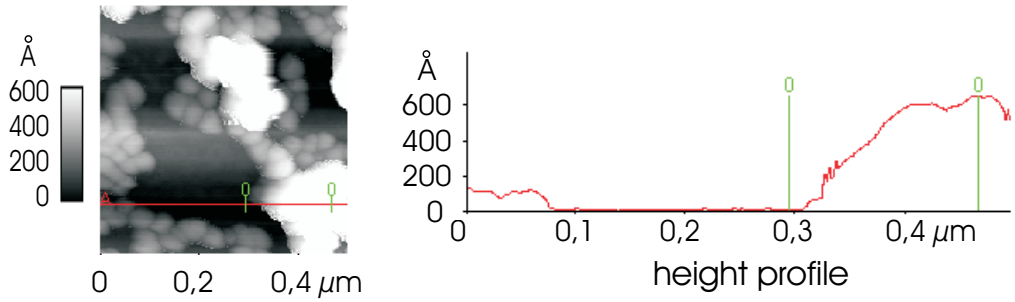

Figure 8. AFM images of gold nanoparticles on quartz substrates irradiated with 3.57 $\frac{J}{cm^2 \cdot pulse}$ and a corresponding height profile. The image shows clearly an ablation of nanoparticles from the surface and the formation of large aggregates with heights of approximately 60 nm and lateral sizes between 100 nm and 200 nm.

were formed (not shown), similar to the results of Fujiwara et al..[28] The reasons therefore is very probably the intensity profile of the laser beam. Thus, only in areas where the laser intensity is high ablation and coalescence occur and large nanoparticles were created. Both processes are non-selective and cause the overall decrease of the extinction amplitude. But due to the fact, that unchanged nanoparticles remain on the substrate the overall decrease is approximately 10 %, only. It should be noted, that the surface plasmon resonance frequency of large nanoparticles with R_{eq} larger than 50 nm lies in the far infrared[4] and cannot be observed in our extinction measurements.

8. SUMMARY AND CONCLUSION

In this contribution we have presented our results on tailoring the shape and size of supported metal nanoparticles with cw and fs pulsed laser light and compared these results to our former results obtained with ns pulsed laser light.

It turned out, that an effective stabilization of the surface plasmon resonance with cw laser light can be achieved. But due to the low and continuous energy impact heating of all nanoparticles and thus, non-selective manipulation of all nanoparticles in the ensemble occures, leading to the symmetric and relatively broad line width.

In the second set of experiments supported nanoparticle ensembles have been irradiated with fs pulsed laser light, in order to tailor the size of the nanoparticles. After irradiation, narrowing of the line width, indicating tailoring of the nanoparticles has been measured. Additionally an overall decrease of the extinction has been observed. The reasons therefore are induced non-thermal and thermal processes, that cause ablation and coalescence of the nanoparticles and thus non-selective tailoring of the size of metal nanoparticles, also.

A comparison of the results obtained with cw and fs pulsed laser light to our former experiments on tailoring the size and shape of nanoparticles with ns pulsed laser light clearly reveals that best results for tailoring the dimensions of metal nanoparticles can be achieved with ns pulsed laser light.

Acknowledgements.
Financial support by the European Union under contract HPRN-CT-2002-00328 NanoCluster and of the Deutsche Forschungsgemeinschaft is gratefully acknowledged.

REFERENCES

1. V. M. Shalaev, *Optical Properties of Nanostructured Random Media*, Springer, Berlin, 2002.
2. K. H. Meiwes-Broer, *Metal Clusters at Surfaces*, Springer, Berlin, 2000.
3. H. Haberland, *Clusters of Atoms and Molecules I and II*, Springer, Berlin, 1994.
4. U. Kreibig and M. Vollmer, *Optical Properties of Metal Clusters*, Springer, Berlin, 1995.

5. J. Bosbach, C. Hendrich, F. Stietz, T. Vartanyan, and F. Träger *Phys. Rev. Lett.* **89**, pp. 257404–1 – 257404–4, 2002.
6. F. Stietz *Appl. Phys. A* **72**, pp. 381–394, 2001.
7. W. D. Knight, K. Clemenger, W. A. de Heer, and W. A. Saunders *Phys. Rev. B* **31**, pp. 2539–2540, 1995.
8. K. Kneipp, Y. Wang, H. Kneipp, L. T. Perelman, I. Itzkan, R. R. Dasari, and M. S. Feld *Phys. Rev. Lett.* **78**, pp. 1667–1670, 1997.
9. S. Nie and S. R. Emory *Science* **275**, pp. 1102–1106, 1997.
10. G. Chumanov and T. M. Cotton *Proc. SPIE* **3608**, pp. 204–210, 1999.
11. I. Gryczynski, J. Malicka, Y. Shen, Z. Gryczynski, and J. Lakowicz *J. Phys. Chem.* **106**, pp. 2191–2195, 2002.
12. J. Lakowicz, B. Shen, Z. Gryczynski, S. D'Auria, and I. Gryczynski *Biochem. and Biophys. Res. Com.* **286**, pp. 875–879, 2001.
13. J. Lakowicz *Analytical Biochem.* **298**, pp. 1–24, 2001.
14. M. Alschinger, M. Maniak, F. Stietz, T. Vartanyan, and F. Träger *Appl. Phys. B.* **76**, pp. 771–774, 2003.
15. R. F. Haglund Jr., L. Yang, R. M. III, J. E. Wittig, K. Becker, and R. A. Zuhr *Opt. Lett.* **18**, pp. 373–375, 1993.
16. S. A. Maier, M. L. Brongerma, P. G. Kik, S. Meltzer, A. A. G. Requicha, and H. A. Atwater *Adv. Mater.* **13**, pp. 1501–1505, 2001.
17. J. Krenn, H. Ditlbacher, G. Schider, A. Hohenau, A. Leitner, and F. R. Aussenegg *J. of Microscopy* **209**, pp. 167–172, 2003.
18. J. Krenn *Nature Materials* **2**, pp. 210–211, 2003.
19. S. A. Maier, P. G. Kik, H. A. Atwater, S. Meltzer, E. Harel, B. K. Koel, and A. A. G. Requicha *Nature Mater.* **2**, pp. 229–232, 2003.
20. J. Bosbach, D. Martin, F. Stietz, T. Wenzel, and F. Träger *Appl. Phys. Lett.* **74**, pp. 2605–2607, 1999.
21. T. Wenzel, J. Bosbach, A. Goldmann, F. Stietz, and F. Träger *Appl. Phys. B* **69**, pp. 513–517, 1999.
22. S. Inasawa, M. Sugiyama, and Y. Yamaguchi *J. Phys. Chem. B* **109**, pp. 3104–3111, 2005.
23. C. M. Aguirre, C. E. Moran, J. F. Young, and N. J. Halas *J. Phys. Chem. B* **108**, pp. 7040–7045, 2004.
24. J. Qiu, X. Jiang, C. Zhu, M. Shirai, J. Si, N. Jiang, and K. Hirao *Angew. Chem.* **116**, pp. 2280–2284, 2004.
25. F. Gonella, G. Mattei, P. Mazzoldi, E. Cattaruzza, G. W. Arnold, G. Battaglin, P. Calvelli, R. Polloni, R. Bertoncello, and R. F. Haglung Jr. *Appl. Phys. Lett.* **69**, pp. 3101–3103, 1996.
26. J. H. Hodak, A. Henglein, M. Giersig, and G. V. Hartland *J. Phys. Chem. B* **104**, pp. 11708–11718, 2000.
27. S. Link, C. Burda, M. B.Mohamed, B. Nikoobakht, and M. A. El-Sayed *Phys. Chem. A* **103**, pp. 1166–1170, 1999.
28. H. Fujiwara, S. Yanagida, and P. V. Kamat *J. Phys. Chem. B* **103**, pp. 2589–2591, 1999.
29. S. Link, C. Burda, B. Nikoobakht, and M. A. El-Sayed *J. Phys. Chem. B* **104**, pp. 6152–6163, 2000.
30. M. Kaempfe, H. Hofmeister, S. Hopfe, G. Seifert, and H. Graener *J. Phys. Chem. B* **104**, pp. 11847–11852, 2000.
31. G. Seifert, M. Kaempfe, K.-J. Berg, and H. Graener *Appl. Phys. B* **73**, pp. 355–359, 2001.
32. V. P. Safonov, V. M. Shalaev, V. A. Markel, Y. E. Danilova, N. N. Lepeshkin, W. Kim, S. G. Rautian, and R. L. Armstrong *Phys. Rev. Lett.* **80**, pp. 1102–1105, 1998.
33. F. Hubenthal, C. Hendrich, H. Ouacha, D. Blázquez Sánchez, and F. Träger *Intern. J. Mod. Phys. B* , eccepted.
34. J. Bosbach, C. Hendrich, F. Stietz, T. Vartanyan, T. Wenzel, and F. Träger *Proc. SPIE* **4274**, pp. 1–8, 2001.
35. F. Stietz, J. Bosbach, T. Wenzel, T. Vartanyan, A. Goldmann, and F. Träger *Phys. Rev. Lett.* **84**, pp. 5644–4647, 2000.
36. T. Wenzel, J. Bosbach, F. Stietz, and F. Träger *Surf. Sci.* **432**, pp. 257–264, 1999.
37. P. B. Johnson and R. W. Christy *Phys. Rev. B* **6**, pp. 4370–4379, 1972.
38. C. Sönnichsen, T. Franzl, T. Wilk, G. von Plessen, J. Feldmann, O. Wilson, and P. Mulvaney *Phys. Rev. Lett.* **88**, pp. 077402–1 – 077402–4, 2002.

39. T. Ziegler, C. Hendrich, F. Hubenthal, T. Vartanyan, and F. Träger *Chem. Phys. Lett.* **386**, pp. 319–324, 2004.
40. F. Hubenthal, T. Ziegler, C. Hendrich, T. Vartanyan, and F. Träger *Proc. SPIE* **5221**, pp. 29–40, 2003.
41. C. Hendrich, J. Bosbach, F. Stietz, F. Hubenthal, and F. Träger *Appl. Phys. B* **76**, pp. 869–875, 2003.
42. D. Edward and I. Palik, *Handbook of Optical Constants of Solids*, Academic Press, New York, 1983.
43. T. Vartanyan, J. Bosbach, F. Stietz, and F. Träger *Appl. Phys. B* **73**, pp. 391–399, 2001.
44. P.-G. Reinhard, M. Brack, F. Calvayrac, C. Kohl, S. Kümmel, E. Suraud, and C. A. Ullrich *Eur. Phys. J. D* **9**, pp. 111–117, 1999.
45. M. Kaempfe, H. Graener, A. Kiesow, and A. Heilmann *Appl. Phys. Lett.* **79**, pp. 1876–1878, 2001.
46. C. Voisin, N. Del Fatti, D. Christofilos, and F. Vallée *J. Chem. Phys. B* **105**, pp. 2264–2280, 2001.
47. S. Stagira, M. Nisoli, S. De Silvestri, A. Stella, P. Tognini, P. Cheyssac, and R. Kofman *Chem. Phys.* **251**, pp. 259–267, 2000.
48. N. Del Fatti, F. Vallée, C. Flytzanis, Y. Hamanaka, and A. Nakamura *Chem. Phys.* **251**, pp. 215–226, 2000.
49. N. Del Fatti, C. Voisin, F. Chevy, F. Vallée, and C. Flytzanis *J. Chem. Phys.* **110**, pp. 11484–11487, 1999.